Cell Reports, Volume *18*

Supplemental Information

Reduced Insulin/IGF-1 Signaling Restores the Dynamic Properties of Key Stress Granule Proteins during Aging

Marie C. Lechler, Emily D. Crawford, Nicole Groh, Katja Widmaier, Raimund Jung, Janine Kirstein, Jonathan C. Trinidad, Alma L. Burlingame, and Della C. David

Figure S1

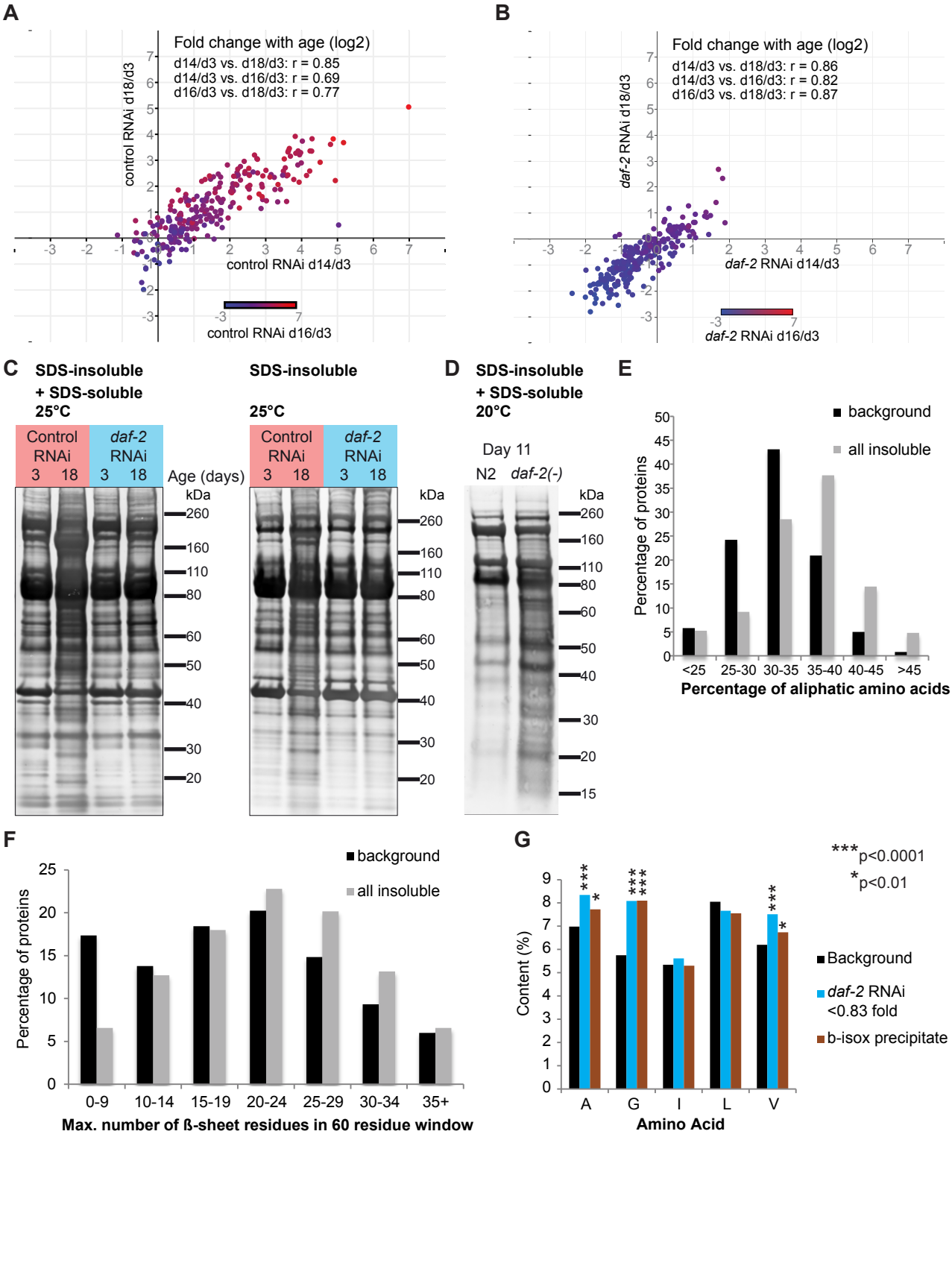
A
Fold change with age (log2)
d14/d3 vs. d18/d3: r = 0.85
d14/d3 vs. d16/d3: r = 0.69
d16/d3 vs. d18/d3: r = 0.77
control RNAi d18/d3
control RNAi d14/d3
control RNAi d16/d3
B
Fold change with age (log2)
d14/d3 vs. d18/d3: r = 0.86
d14/d3 vs. d16/d3: r = 0.82
d16/d3 vs. d18/d3: r = 0.87
daf-2 RNAi d18/d3
daf-2 RNAi d14/d3
daf-2 RNAi d16/d3
C
SDS-insoluble
+ SDS-soluble
25°C
Control RNAi
daf-2 RNAi
3 18 3 18
Age (days)
kDa
260
160
110
80
60
50
40
30
20
SDS-insoluble
25°C
D
SDS-insoluble
+ SDS-soluble
20°C
Day 11
N2 daf-2(-)
E
background
all insoluble
Percentage of proteins
<25 25-30 30-35 35-40 40-45 >45
Percentage of aliphatic amino acids
F
background
all insoluble
Percentage of proteins
0-9 10-14 15-19 20-24 25-29 30-34 35+
Max. number of ß-sheet residues in 60 residue window
G
***p<0.0001
*p<0.01
Background
daf-2 RNAi <0.83 fold
b-isox precipitate
Content (%)
A G I L V
Amino Acid

Figure S1. Changes in insolubility with age are highly correlated between the three biological replicates. Related to Figure 1.

(A) Fold changes in insolubility with age in animals treated with control RNAi are plotted for three biological replicates. Spearman r correlation r= 0.77 d18/d3 versus d16/d3, r= 0.85 d18/d3 versus d14/d3 and r= 0.67 d14/d3 versus d16/d3; two-tailed p-value p<0.0001 d18/d3 versus d16/d3, p<0.0001 d18/d3 versus d14/d3 and p<0.0001 d14/d3 versus d16/d3.

(B) Fold changes in insolubility with age in animals treated with *daf-2* RNAi are plotted for three biological replicates. Spearman r correlation r= 0.87 d18/d3 versus d16/d3, r= 0.86 d18/d3 versus d14/d3 and r= 0.82 d14/d3 versus d16/d3; two-tailed p-value p<0.0001 d18/d3 versus d16/d3, p<0.0001 d18/d3 versus d14/d3 and p<0.0001 d14/d3 versus d16/d3.

(C) Sypro Ruby whole protein staining of [SDS-soluble + SDS-insoluble] fraction and SDS-insoluble fraction from day 3 and day 18 *gon-2(-)* mutants exposed to control and *daf-2* RNAi (grown at 25°C).

(D) Sypro Ruby whole protein staining of [SDS-soluble + SDS-insoluble] fraction from aged (day 11) wildtype (N2) and *daf-2(-)* mutants (grown at 20°C).

(E) Aggregation-prone proteins (all insoluble proteins, n= 228) are enriched in aliphatic amino acids.
Unequal variance t-test: p= 3.7E-14.

(F) Aggregation-prone proteins (all insoluble proteins, n= 228) are enriched in extended stretches of β-sheet propensity. Unequal variance t-test: p= 7.9E-7.

(G) Alanine, glycine and valine are significantly enriched in aggregation-prone proteins selectively targeted by long-lived *daf-2(-)* animals compared to the background proteome (<0.83 fold change in aggregation in *daf-2(-)* conditions, n= 81, unequal variance t test: A, p= 9.6E-5, G, p= 1.1E-5, V, p= 1.3E-6). Similarly, these three amino acids are enriched in proteins precipitated by b-isox (n= 126, unequal variance t test: A, p= 0.007, G, p= 8.8E-9, V, p= 0.004).

Figure S2

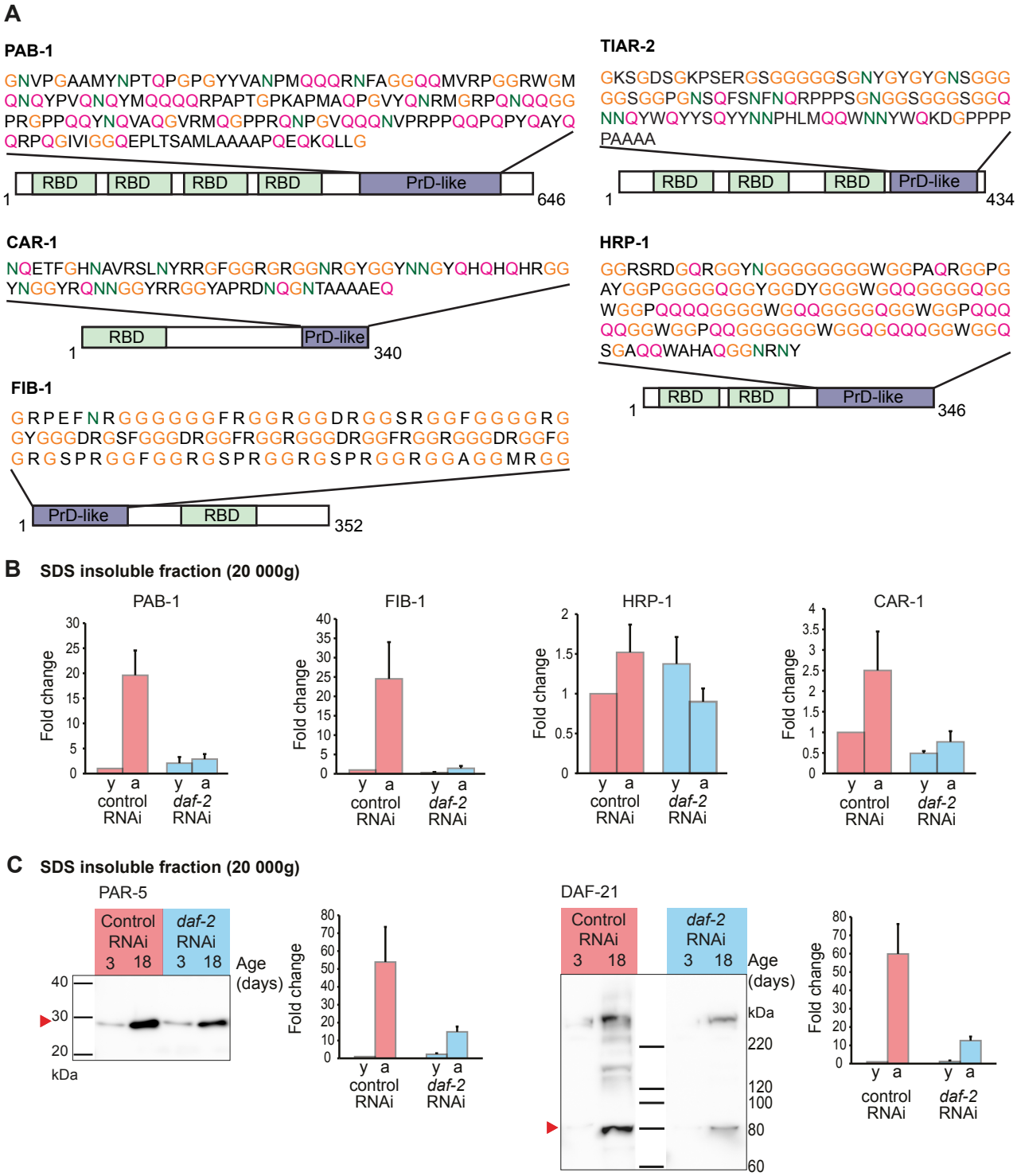

Figure S2: Reduced *daf-2* signaling efficiently prevents age-dependent insolubility of RBP with LC "prion-like" domains. Related to Figure 1.

(A) Graphical depiction of PAB-1, TIAR-2, HRP-1, CAR-1 and FIB-1. Green boxes represent RNA-binding domains (RBD) and purple boxes prion-like LC domains (PrD-like). Amino acid sequences of PrDs are detailed. Amino acids enriched in PrD-like domains: glycines, glutamines and asparagines are coloured.

(B) Quantifications of immunoblots detecting RBPs PAB-1, FIB-1, HRP-1 and CAR-1 in the SDS-insoluble fraction. The averages of three biological replicates ± SEM are represented.

(C) Relevant protein bands indicated by red arrow. Quantifications of immunoblots detecting PAR-5 and DAF-21 in the SDS-insoluble fraction. The averages of three biological replicates ± SEM are represented.

Figure S3

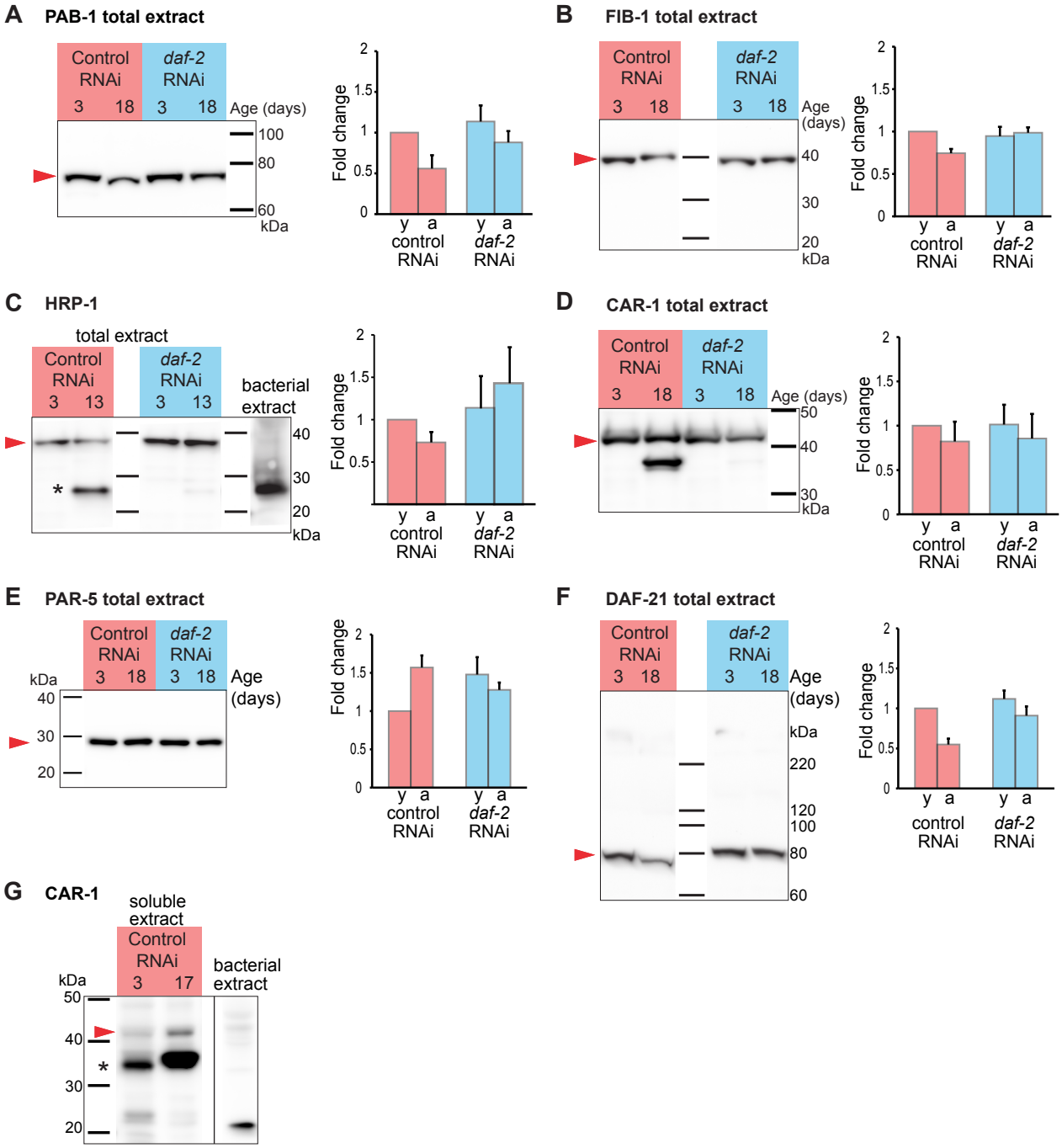

Figure S3. Total protein levels do not change upon *daf-2* inhibition. Related to Figure 1.
(A) Immunoblot of PAB-1 (red arrow) in the total extract.
(B) Immunoblot of FIB-1 (red arrow) in the total extract.
(C) Immunoblot of HRP-1 (red arrow) in the total extract. Truncated band between 20 and 30kDa (marked by asterisk) detected by anti-HRP-1 is due to cross-reaction with bacterial protein.
(D) Immunoblot of CAR-1 (red arrow) in the total extract.
(E) Immunoblot of PAR-5 (red arrow) in the total extract.
(F) Immunoblot of DAF-21 (red arrow) in the total extract.
(G) Truncated band between 30 and 40kDa (marked by asterisk) detected by anti-CAR-1 is not present in bacterial sample.
Quantifications represent the average of three biological replicates ± SEM. For the quantifications, total band levels were normalized to total protein levels detected by Sypro Ruby.

Figure S4

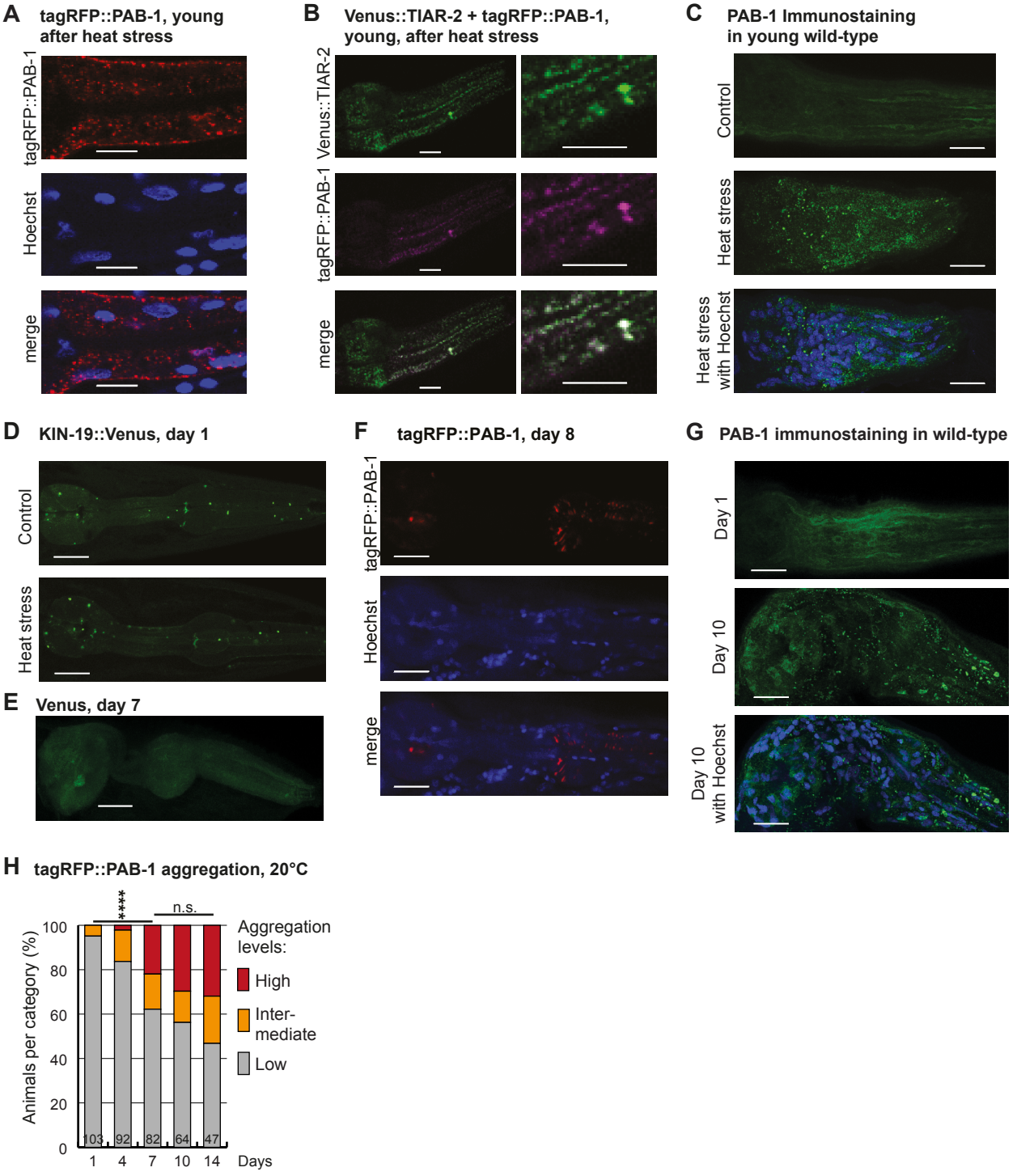
A
tagRFP::PAB-1, young after heat stress
tagRFP::PAB-1
Hoechst
merge
B
Venus::TIAR-2 + tagRFP::PAB-1, young, after heat stress
Venus::TIAR-2
tagRFP::PAB-1
merge
C
PAB-1 Immunostaining in young wild-type
Control
Heat stress
Heat stress with Hoechst
D
KIN-19::Venus, day 1
Control
Heat stress
E
Venus, day 7
F
tagRFP::PAB-1, day 8
tagRFP::PAB-1
Hoechst
merge
G
PAB-1 immunostaining in wild-type
Day 1
Day 10
Day 10 with Hoechst
H
tagRFP::PAB-1 aggregation, 20°C
****
n.s.
Animals per category (%)
100
80
60
40
20
0
103
92
82
64
47
1
4
7
10
14
Days
Aggregation levels:
High
Inter-mediate
Low

Figure S4. PAB-1 accumulates in puncta with age in wildtype *C. elegans*. Related to Figure 2.

(A) Zoom into the procorpus of tagRFP::PAB-1 expressed in the pharyngeal muscles showing cytoplasmic and nuclear tagRFP::PAB-1 stress granules upon heat stress (2h, 32°C) at day 1 of adulthood. Representative single plane confocal images. Scale bar 7µm.

(B) tagRFP::PAB-1 and Venus::TIAR-2 co-localize in stress granules upon heat stress (2h, 32°C). Experiment performed at day 2 of adulthood. Scale bar 7µm.

(C) Exposure to 35°C for 3h in wildtype N2 animals at day 1 leads to stress granule formation detected by PAB-1 antibody. Scale bar 15µm.

(D) KIN-19::Venus does not form stress granules after exposure to heat stress (32°C, 2h) as seen in the pharynx of worms expressing *Pkin-19::KIN-19::Venus* at day 1. Scale bar 15µm.

(E) Venus-tag alone does not aggregate with age in animals expressing *Pmyo2::Venus*, day 7. Scale bar 15µm.

(F) Animals expressing *Pmyo-2::tagRFP::PAB-1* at day 8 show cytoplasmic tagRFP::PAB-1 puncta. Representative single plane confocal images. Scale bar 15µm.

(G) Immunostaining of PAB-1 in the head region of wildtype N2 worms reveals a diffuse PAB-1 pattern at day 1 which changes into a punctate pattern at day 10. Scale bar 15µm.

(H) After day 7 of adulthood the increase in tagRFP::PAB-1 aggregation with age in *Pmyo-2::tagRFP::PAB-1* transgenics is not significant. Day 1 versus day 7: ****p<0.0001, day 7 versus day 14: n.s.=0.0999.

Figure S5

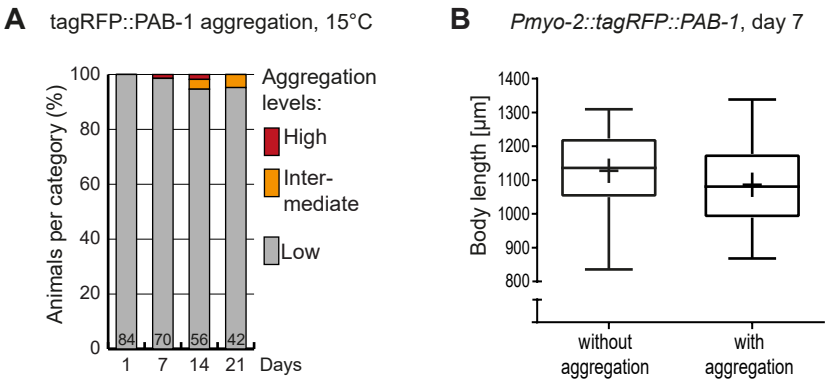

Figure S5. Age-dependent PAB-1 aggregation is associated with reduced body size. Related to Figure 4.
(A) No significant increase of tagRFP::PAB-1 aggregation in *Pmyo-2::tagRFP::PAB-1* transgenics grown at 15°C. At all ages $p>0.05$.
(B) Animals with tagRFP::PAB-1 aggregation are significantly smaller than animals without aggregation (biological repeat, day 7, $p=0.0041$). Data represented with Tukey-style box plots and mean indicated by + (animals without aggregation N = 100, with aggregation N = 149).

Figure S6

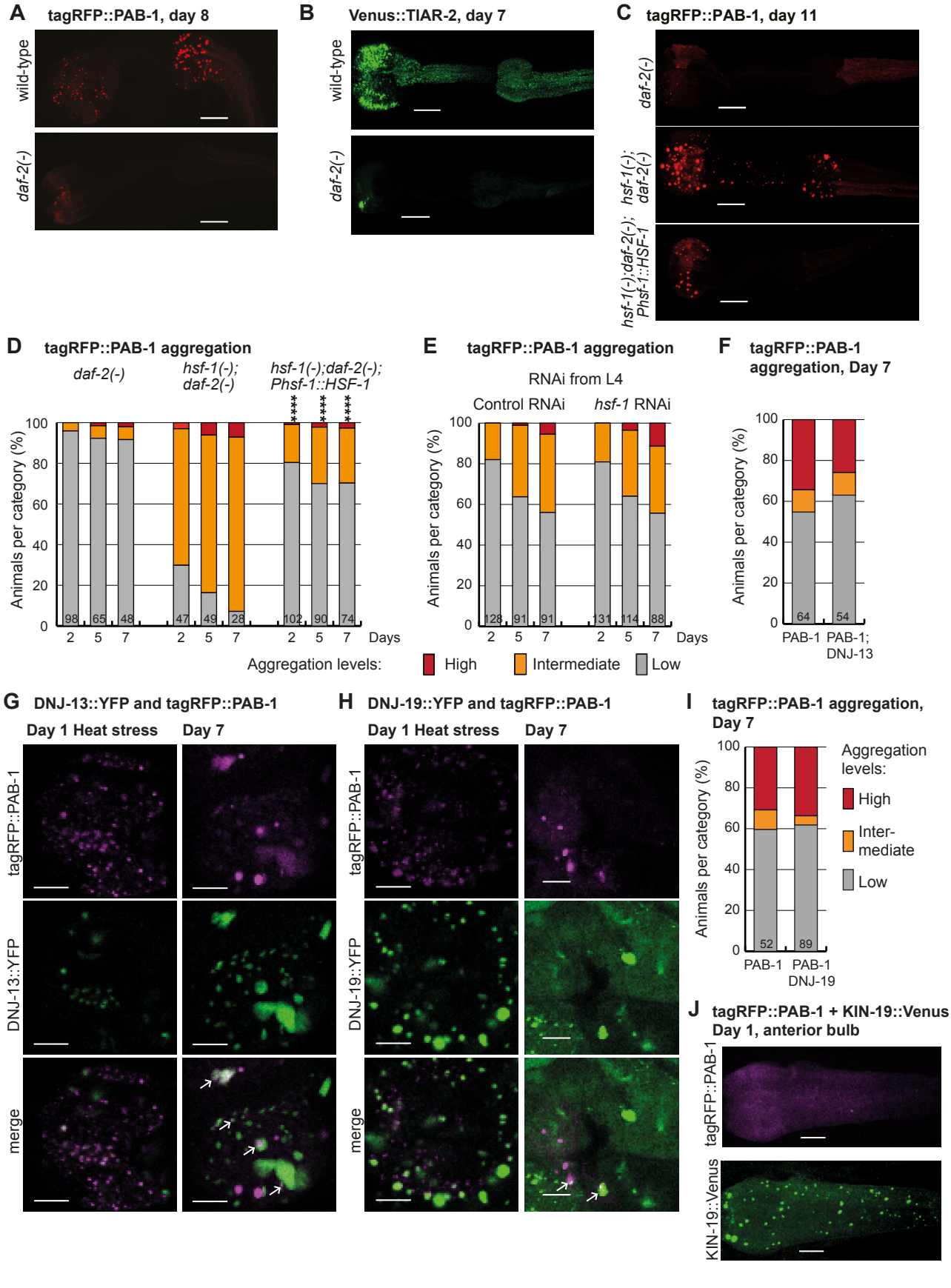
A
tagRFP::PAB-1, day 8
wild-type
daf-2(-)
B
Venus::TIAR-2, day 7
wild-type
daf-2(-)
C
tagRFP::PAB-1, day 11
daf-2(-)
hsf-1(-); daf-2(-)
hsf-1(-);daf-2(-); Phsf-1::HSF-1
D
tagRFP::PAB-1 aggregation
daf-2(-)
hsf-1(-); daf-2(-)
hsf-1(-);daf-2(-); Phsf-1::HSF-1
****
Animals per category (%)
100
80
60
40
20
0
98 65 48 47 49 28 102 90 74
2 5 7 2 5 7 2 5 7
Days
Aggregation levels:
High
Intermediate
Low
E
tagRFP::PAB-1 aggregation
RNAi from L4
Control RNAi
hsf-1 RNAi
Animals per category (%)
128 91 91 131 114 88
2 5 7 2 5 7
Days
F
tagRFP::PAB-1 aggregation, Day 7
Animals per category (%)
64 54
PAB-1
PAB-1; DNJ-13
G
DNJ-13::YFP and tagRFP::PAB-1
Day 1 Heat stress
Day 7
tagRFP::PAB-1
DNJ-13::YFP
merge
H
DNJ-19::YFP and tagRFP::PAB-1
Day 1 Heat stress
Day 7
tagRFP::PAB-1
DNJ-19::YFP
merge
I
tagRFP::PAB-1 aggregation, Day 7
Animals per category (%)
52 89
PAB-1
PAB-1 DNJ-19
Aggregation levels:
High
Inter-mediate
Low
J
tagRFP::PAB-1 + KIN-19::Venus
Day 1, anterior bulb
tagRFP::PAB-1
KIN-19::Venus

Figure S6. Colocalization of chaperones DNJ-13 and DNJ-19 with PAB-1 stress granules and age-dependent puncta does not influence PAB-1 aggregation levels. Related to Figure 5.
(A) *daf-2* mutants prevent tagRFP::PAB-1 puncta formation. Scale bar 15μm.
(B) *daf-2* mutants prevent Venus::TIAR-2 puncta formation. Scale bar 15μm.
(C) HSF-1 overexpression stops increased tagRFP::PAB-1 aggregation in day 11 *Pmyo-2::tagRFP::PAB-1* transgenics in the *hsf-1; daf-2* double mutant background. Scale bar 15μm.
(D) HSF-1 overexpression rescues effect of *hsf-1* mutation in *daf-2* mutant background. Day 2, day 5 and day 7, versus *hsf-1(-);daf-2(-)*,****p<0.0001.
(E) HSF-1 knockdown after development is not sufficient to delay tagRFP::PAB-1 aggregation. L4440 empty vector used as RNAi control. Fisher's exact test two-tailed not significant.
(F) No significant change in tagRFP::PAB-1 aggregation with age by DNJ-13::YFP overexpression in a population of *C. elegans* at day 7 (p>0.05).
(G) tagRFP::PAB-1 and DNJ-13::YFP colocalize in heat stress induced stress granules and age-related puncta. Arrows mark colocalization of chaperones with age-related puncta. Representative single plane images. Scale bar 5μm.
(H) tagRFP::PAB-1 and DNJ-19::YFP colocalize in heat stress induced stress granules and age-related puncta. Arrows mark colocalization of chaperones with age-related puncta. Representative single plane images. Scale bar 5μm.
(I) No significant change in tagRFP::PAB-1 aggregation with age by DNJ-19::YFP overexpression in a population of *C. elegans* at day 7 (p>0.05).
(J) KIN-19::Venus expression does not induce widespread PAB-1 stress granule formation. Scale bar 7μm.

Supplemental tables:

Table S1: Long-lived *C. elegans* with reduced insulin/IGF-1 signaling efficiently prevent protein insolubility with age. Related to Figure 1.

In category "Control RNAi aged/young" bold highlights insoluble proteins with more than 2 fold accumulation with age in control conditions. In category "*daf-2* RNAi aged/young" bold highlights proteins which aggregate with age in *daf-2(-)* conditions (>1.2 fold), underlined highlights proteins with reduced aggregation with age in *daf-2(-)* conditions (<0.83 fold).

Table S2. Functional annotation of age-dependent protein insolubility modulated by reduced *daf-2* signaling. Related to Figure 1.

(A) RNA-binding proteins are over-represented among the proteins which are protected from aggregation in the long-lived *daf-2(-)* animals

Gene ontology or SP-PIR Keyword	Number of proteins	% of total	*p* Value
Ribosomal protein	32	37.6	1.6E-39
Growth	45	52.9	3.2E-10
RNA-binding	10	11.8	6.6E-07
Muscle proteins	4	4.7	3.1E-04
Determination of adult life span	11	12.9	8.5E-04
Generation of precursor metabolites and energy	7	8.2	0.009

Functional annotation of the protein set which aggregated less with age in *daf-2(-)* conditions was carried out using the DAVID software. A total of 85 out of 87 aggregated proteins were recognized by DAVID. Enrichment in GOTERM_BP_FAT and SP_PIR_KEYWORDS were evaluated. EASE score p value: modified Fisher Exact p-value.

(B) Chaperones and yolk proteins are over-represented among proteins which are still prone to aggregate in long-lived *daf-2(-)* animals

Gene ontology or SP-PIR Keyword	Number of proteins	% of total	*p* Value
Stress response	7	14	6.4E-08
(7 Chaperones)			
Secreted	7	14	7.3E-06
(5 Vitellogenins)			
Determination of adult life span	7	14	0.002

Functional annotation of the protein set which continued to aggregate with age in *daf-2(-)* conditions was carried out using the DAVID software. A total of 50 out of 52 aggregated proteins were recognized by DAVID. Enrichment in GOTERM_BP_FAT and SP_PIR_KEYWORDS were evaluated. EASE score p value: modified Fisher Exact p-value.

Table S3. RNA-binding proteins protected from aggregation in the long-lived *daf-2(-)* animals. Related to Figure 1.

Uniprot KB	Gene name	Protein name	Prion-like domain*	Stress granule[#]	P-granule[$]
P27639	*inf-1*	Eukaryotic initiation factor 4A		yes	
P34563	*iff-1*	Eukaryotic translation initiation factor 5A-1		yes	
Q19072	*tufm-1*	Elongation factor Tu		yes	
P53013	*eft-3*	Elongation factor 1-alpha		yes	
O16520	*erfa-1*	Eukaryotic peptide chain release factor subunit 1			
Q22037	*hrp-1*	Heterogeneous nuclear ribonucleoprotein A1	yes	yes	
Q9U302	*pab-1*	Polyadenylate-binding protein	yes	yes	yes
Q9XW17	*car-1*	CAR-1	yes	yes	yes
Q9XTJ6	*cey-4*	CEY-4		yes	yes
P34689	*glh-1*	ATP-dependent RNA helicase glh-1			yes
Q22053	*fib-1*	rRNA 2'-O-methyltransferase fibrillarin	yes		

(*) RNA-binding proteins containing prion-like domains as determined by the algorithm developed by Alberti et al. 2009.

([#],[$]) RNA-binding proteins previously shown to localize to stress granules or P-granules in the literature (including references to their homologs in other organisms).

Table S4: Proteins precipitated by b-isox are prone to aggregate with age in *C. elegans* and not in long-lived *daf-2(-)* conditions. Related to Figure 1.

Table S5: Lifespan analysis of *pmyo-2::tagRFP::PAB-1* transgenics. Related to Figure 4.

Temperature	Transgenics	Mean lifespan (Days)	Age at 75% mortility (days)	Number of transgenic animals	Censored	P-value
15°C	wildtype	24.12	28	103	19	
	pmyo-2::tagRFP::PAB-1	31.44	35	100	38	<0.0001
20°C	wildtype	19.37	22	100	18	
	pmyo-2::tagRFP::PAB-1	23.62	27	101	23	<0.0001
25°C	wildtype	9.22	12	100	12	
	pmyo-2::tagRFP::PAB-1	14.06	17	99	31	<0.0001
20°C, 25°C from day 7 Repeat 1	*pmyo-2::tagRFP::PAB-1* low+medium aggregation	19.66	21	159	35	
	pmyo-2::tagRFP::PAB-1 high aggregation	18.54	21	60	4	0.029
20°C, 25°C from day 7 Repeat 2	*pmyo-2::tagRFP::PAB-1* low+medium aggregation	18.26	21	129	12	
	pmyo-2::tagRFP::PAB-1 high aggregation	18.53	21	31	5	0.562
20°C, 25°C from day 7 Repeat 3	*pmyo-2::tagRFP::PAB-1* low+medium aggregation	19.04	21	112	62	
	pmyo-2::tagRFP::PAB-1 high aggregation	15.73	17	25	2	<0.0001
20°C, 25°C from day 7 Repeat 4	*pmyo-2::tagRFP::PAB-1* low+medium aggregation	20.62	23	228	44	
	pmyo-2::tagRFP::PAB-1 high aggregation	19.42	22	89	5	0.030
20°C, sorted at day 7	*pmyo-2::tagRFP::PAB-1* low+medium aggregation	21.73	24	155	24	
	pmyo-2::tagRFP::PAB-1 high aggregation	20.64	24	89	16	0.028

Table S6: RNAi targeting of HSP-70 does not affect PAB-1 aggregation rates. Related to Figure 5.

	Repeat 1				Repeat 2			
	Day 1		Day 2		Day 1		Day 2	
Aggregation levels	Control	HSP-70	Control	HSP-70	Control	HSP-70	Control	HSP-70
Low	90	77	80	79	93	94	77	64
Intermediate	12	22	19	17	7	5	8	12
High	2	1	6	6	4	3	9	13

Number of animals with categories of tagRFP::PAB-1 aggregation: low (<10 tagRFP::PAB-1 puncta), intermediate (>10 tagRFP::PAB-1 puncta in posterior bulb), high (>10 tagRFP::PAB-1 puncta in anterior bulb). Empty vector control or RNAi targeting HSP-70 (CELE_C12C8.1).

Supplemental movies:

Movie S1. Smaller animals with PAB-1 aggregates are less motile. Related to Figure 4

Pmyo-2::tagRFP::PAB-1 animals grown at 20°C until day 7 before transfer to 25°C until day 10. Representative small (775µm) and big (1257 µm) worms were filmed at day 10.

Supplemental Experimental Procedures:

Strains:
Wild type: N2
CF2253: *gon-2(q388) I (outcrossed 4x)*
CF1041: *daf-2(e1370) III*

Transgenics:
CF3706: N2; *muEx587[Pkin-19::kin-19::mEOS2+Punc-122::gfp]*
DCD101: *hsf-1(sy441) I; daf-2(e1370) III; uqIs24[Pmyo-2::tagrfp::pab-1]*
DCD179: N2*; uqEx37[Pkin19::kin19::venus + Punc-122::gfp]*
DCD194: N2; *uqEx41[Pmyo-2::venus::tiar-2]*
DCD214: N2; *uqIs24[Pmyo-2::tagrfp::pab-1]*
DCD215: *daf-2(e1370) III; uqIs24[Pmyo-2::tagrfp::pab-1]*
DCD217: N2; *uqIs24[Pmyo-2::tagrfp::pab-1]; uqEx37[Pkin-19::kin-19::venus + Punc-122::gfp]*
DCD219: N2; *uqIs24[Pmyo-2::tagrfp::pab-1]; uqEx41[Pmyo-2::venus::tiar-2]*
DCD236: *daf-16(mu86) I; daf-2(e1370) III; uqIs24[Pmyo-2::tagrfp::pab-1]*
DCD249: *hsf-1(sy441) I; uqIs24[Pmyo-2::tagrfp::pab-1]*
DCD250: *daf-2(e1370)III; uqEx41[Pmyo-2::venus::tiar-2]*
DCD253: *eat-2(ad1116)II;uqIs24[Pmyo-2::tagrfp::pab-1]*
DCD256: *hsf-1(sy441)I; daf-2(e1370)III; uqIs24[Pmyo-2::tagrfp::pab-1]; muIs115[Phsf-1::hsf-1 + Pmyo-3::GFP]*
DCD284: N2; *uqIs24[Pmyo-2::tagrfp::pab-1]; uqEx49[pkin-19::meos]*
DCD287: N2; *uqIs24[Pmyo-2::tagrfp::pab-1]; uqIs1[pdnj-13::dnj-13::yfp]*
DCD288: N2; *uqIs24[Pmyo-2::tagrfp::pab-1]; uqIs2[pdnj-19::dnj-19::yfp]*

Maintenance:
All strains were maintained at 15°C by standard techniques on NGM plates seeded with OP50. Day 1 of adulthood is defined as 24h after the last larval stage L4. Before each experiment, adults of the desired strains were transferred to 20°C and their progeny selected at L4 stage to achieve synchronization. For experiments with worms carrying mutations as well as DCD212, DCD226, DCD194, DCD219 strains, the adults were maintained at 15°C, their progeny picked at L4 stage and thereafter transferred to 20°C.

Lifespan analysis:
Worms were grown on OP50 seeded NGM plates at the experimental temperature indicated and were scored every day for live animals, dead animals (no longer responding to body touch) and censored animals (crawled off plates, contaminated, ruptured or showing internal hatching). For lifespan analysis under mild stress, worms were grown at 20°C and transferred to 25°C at day 7. Survival analyses were performed using the Kaplan-Meier method using an online application for survival analysis (Yang et al., 2011).

Movie acquisition:
Movies were taken for 60 seconds of worms on NGM plates without bacteria using a Leica M165 FC microscope with a Planapo 2.0x objective and a Leica DFC310 FX camera. The videos were modified to play side by side at double playing speed using Vidiot software (https://sourceforge.net/projects/vidiot/).

RNAi treatment:
RNAi by feeding was performed as described previously (Hansen et al., 2005). All RNAi clones were obtained from the Marc Vidal RNAi feeding library or the Julie Ahringer RNAi feeding library (Source BioScience, UK) and sequenced. HT115 containing the empty vector L4440 was used as control.

Cloning and Strain Generation:
Cloning was carried out using the Gateway system (Life Technologies, Darmstadt, Germany). *Pmyo-2* promoter was kindly provided by Brian Lee, UCSF. *tiar-2* cDNA was amplified from a cDNA library prepared from total RNA isolated from N2 worms. The *pab-1* gene was amplified from N2 total DNA extract. All constructs contain the *unc-54* 3′ UTR. The tagrfp vector was obtained from Evrogen (AXXORA, San Diego, CA, USA). Venus was generated by targeted mutation of the *yfp* gene. Constructs were generated with fluorescent tags inserted either before or after the gene to avoid disrupting LC domain. Constructs were sequenced at each step. *Pmyo-2::tagrfp::pab-1* was injected at 10 ng/µl (whole plasmid injected), *Pkin-19::kin-19::venus* at 30ng/µl together with the coinjection marker *Punc-122::gfp* at 100ng/µl (whole plasmids injected). Undiluted PCR amplified

Pmyo-2::venus::tiar-2 was injected at 10 ng/µl to generate transgenics. All constructs were injected into N2 animals. To avoid the vector backbone, constructs were amplified by PCR with the following primers: Primer 1 (T3) ATTAACCCTCACTAAAGGGA and primer 2 TTAAGTTGGGTAACGCCAGG. Stable lines expressing PAB-1 were generated by irradiating the animals containing the extrachromosomal array in a CL-1000 Ultraviolet Crosslinker (UVP) with 275µJ x 100. 100% transmission line was backcrossed four times into the wild-type N2 strain. Non-integrated strains expressing DNJ-13::YFP and DNJ-19::YFP were obtained from Klaus Richter (Papsdorf et al., 2014) and integrated by gamma irradiation following standard procedures. These strains were then backcrossed three times into the wild-type N2 strain.

Imaging and immunofluorescence staining:
Fixation protocols for direct confocal analysis or immunohistochemistry were adapted from a fixation protocol previously described (Antibody Staining of *C. elegans* by Michael Koelle, https://medicine.yale.edu/lab/koelle/protocols/Antibody%20Staining_180540_21947.pdf). Worms at the desired age and after treatment were picked into M9 containing OP50 and then washed once with H_2O before being resuspended in fixation solution containing 1% PFA. After mixing thoroughly, worms were immediately immersed into liquid nitrogen for freezing. Tubes were thawed at 70°C and refrozen in dry ice two times and then rotated overnight at 4°C. For direct confocal analysis worms were washed hereafter with PBST-B and optionally stained with Hoechst33342 stain (NucBlue Live Cell Stain Ready Probes Reagent, Life Technologies) for 20 minutes before washing again and mounting them on slides using Fluorescent Mounting Medium (Dako). For immunohistochemistry, worms were permeabilized and stained as previously described using PAB-1 antibody (1:200, (Scheckel et al., 2012)) and AlexaFluor488 conjugated anti-rabbit (Invitrogen) diluted 1:200 as secondary antibody. Worms were stained with Hoechst33342 for 20 minutes and placed on a slide using Fluorescent Mounting Medium (Dako).
Worms were examined under a Leica SP8 confocal microscope with the HC PL APO CS2 63x1.40 oil objective using the Leica HyD hybrid detector. In single transgenics, tagRFP was detected using 555nm as excitation and an emission range from 560-650nm, Venus with 514nm as excitation wavelength and an emission range from 520-570nm. In double transgenic animals emission ranges were narrowed to 570-600nm for tagRFP and 521-551nm for Venus to prevent detection of cross-emission. Hoechst33342 staining was visualized with an excitation of 405nm and an emission range from 430-500nm. Alexa Fluor488 antibody was excited with 488nm and detected with an emission range from 500-550nm. 3D reconstructions were performed using the Leica Application Suite (LAS X). Puncta size of single plane images was determined using Fiji software (Schindelin et al., 2012).

FRAP analysis:
FRAP analysis was performed as previously described (David et al., 2010) using the Leica SP8 confocal microscope with the HC PL APO CS2 63x 1.30 glycerol objective and PMT detector. Bleach settings: 4x 20% for PAB-1 and TIAR-2 puncta. tagRFP: 555nm excitation, 565-620nm emission. Venus: 514 excitation, 521-551nm emission. Relative fluorescence intensity (RFI) was analyzed as described previously following the equation RFI = (Tt/Ct)/(T0/C0), where T0 is the intensity in the region of interest (ROI) before photobleaching; Tt, the intensity in the ROI at a defined time after photobleaching; C0, the intensity in the non-bleached part of the puncta before photobleaching; and Ct, the intensity in the non-bleached part of the puncta after bleaching (Brignull et al., 2006).

Insoluble protein extraction:
To isolate SDS-insoluble proteins for mass spectrometry analysis, we performed a sequential extraction as previously described (David et al., 2010). 350mg ground worms per treatment were solubilized in two volumes of a high salt RAB buffer (0.1 M MES, 1 mM EGTA, 0.1 mM EDTA, 0.5 mM MgSO4, 0.75 M NaCl, 0.02 M NaF, 1 mM PMSF, Roche Complete Inhibitors 2x, DNaseI and RNaseI). High-salt soluble proteins were removed by centrifugation with 20 000g, 20 minutes at 4°C. The pellet was reextracted in RAB buffer with 1 M sucrose to help remove lipids and then resuspended twice in two volumes of RIPA buffer (50 mM Tris pH 8, 150 mM NaCl, 5 mM EDTA, 0.5% SDS, 0.5% SDO, 1% NP-40, 1 mM PMSF, Roche Complete Inhibitors 1x). Detergent soluble proteins were removed by centrifugation with 20 000g, 20 minutes at 4°C. This final pellet containing highly insoluble proteins was resuspended in 200µl 70% formic acid and centrifuged at 50 000g to remove worm cuticlar debris.
To isolate insoluble proteins for western blot analysis, a simplified protocol was used where 50mg of ground animals in RAB buffer were directly resuspended in 150µl RIPA buffer. SDS-insoluble proteins were isolated by washing with RIPA buffer containing 0.5% SDS and centrifugation with 20 000g for 20 minutes at 4°C. To compare insoluble proteins collected by our method to those collected by Walther et al, we omitted SDS in the RIPA wash thus collecting both SDS-soluble and SDS-insoluble proteins after centrifugation with 500 000g for 10 minutes at 4°C as previously described (Walther et al., 2015). For both extractions, we washed the pellet

once in 100µl RIPA. Final pellets containing insoluble proteins were recovered in 75µl 8 M Urea, 2% SDS, 50 mM DTT, 50 mM Tris pH 7.4 at room temperature.

Insoluble protein extraction using *C. elegans* with gonads:
To investigate the effect of reduced *daf-2* signaling on protein insolubility in animals with gonads, 550 N2 and CF1041 worms were grown at 20°C. Worms were collected at day 1 or day 11 in RAB buffer and homogenized with the Precellys Lysing Kit (Cayman Chemical) using 1.4 mm ceramic beads. After adding the homogenate into tubes without beads and centrifugation at 20,000g for 20 minutes at 4°C, the protein extraction was performed as described in "Insoluble protein extraction". SDS was omitted in the RIPA wash and centrifugations were performed at 20,000g.

Mass spectrometry analysis:
SDS-insoluble proteins dissolved in formic acid were further processed for mass spectrometry analysis as previously described (David et al., 2010). Briefly, after dialysis, proteins were solubilized in final concentration of 8M Urea. After alkylation and reduction, samples were diluted in 150mM ammonium bicarbonate to obtain a final 2M Urea concentration. Proteins were digested by modified trypsin (Promega, Madison, WI) at 5% w/w overnight at 37°C. Peptides from young and aged animals on control and *daf-2* RNAi were labelled by 4-plex iTRAQ following the manufacturer's instructions (Applied Biosystems, Pleasanton, CA, USA). We checked that over 95% of the peptides were labelled with iTRAQ by analysing the sample on a 1-h LC-MS/MS run and searching the spectra, allowing iTRAQ as a variable modification. In order to decrease sample complexity and improve identification, peptides were separated by SCX fractionation and desalted. A total of 46 SCX fractions were collected. Individual SCX fractions were separated on a reverse phase C18 (LC Packings, Sunnyvale, CA) and the LC eluate was coupled to a micro-ionspray source attached to a QSTAR Pulsar Elite mass spectrometer (Applied Biosystems, Foster City, CA) (Trinidad et al., 2013). SCX fractions 1-20 contained relatively few peptides and were analysed by a single LC-MS analysis. To increase the coverage of peptides fractions 21-46 were analysed twice by LC-MS/MS. In the first analysis, only those ions with m/z between 375 and 600 were selected for data-dependent MS/MS, while in the second analysis, this range was between 590 and 1200 Da.
MS/MS spectra were analysed as previously described (David et al., 2010). We kept peptides that had at least one iTRAQ peak area over 25 counts. For proteins identified by one single peptide, peptides with an expectation value larger than 1E-3 were eliminated. For proteins identified by two or more peptides, we discarded peptides with an expectation value larger than 1E-2. The false positive rates were estimated by conducting the search using a concatenated database containing the original UniProt database as well as a version of each original entry where the sequence has been randomized. Using this stringent cut-off, we did not identify any decoy database proteins, indicating that the protein false discovery rate was much less than 1%. In the insoluble fractions, we detected a total of 438 proteins comparing extracts from day16/day3 old animals, 470 proteins comparing extracts from day18/day3 old animals and 492 proteins comparing extracts from day14/day3 old animals. To determine the relative level of each protein, we averaged the ratio of (peak area of sample of interest)/(sum of peak areas from all four conditions) for all peptides identified for each protein. To measure the fold change in levels of aggregation-prone proteins with age, we divided the ratio for aged control or aged *daf-2* RNAi samples by the respective ratio for young control or young *daf-2* RNAi samples. For further data analysis, we kept only proteins present in all three biological replicates and averaged their fold changes.
Calculation of correlations between fold changes in insolubility between the repeats (Figure S1A and S1B) was performed using GraphPad Prism 6 software. Data was tested for normality with D'Agostino & Pearson omnibus normality test and Spearman r correlation was calculated as several data sets did not pass the normality test.

Western blotting analysis:
The following antibodies were used: anti-PAB-1 (1:60, (Scheckel et al., 2012)), anti-HRP-1 (1:200, (Joeng et al., 2004)), anti-CAR-1 (1:400, (Boag et al., 2005)), anti-fibrillarin (1:1000, #2639, Cell Signaling), anti-HSP-90 (1:500, #4874, Cell Signaling) and anti-14-3-3 (1:5000, SC-1657, Santa Cruz Biotechnology). Bands detected by immunoblot or whole lanes detected by Sypro Ruby blot staining (Thermo Scientific) for total protein levels were quantified using Image J.

Bioinformatics analysis:
The *C. elegans* proteome set was prepared by obtaining all proteins identified by mass spectrometry available in PeptideAtlas 2011 (http://www.peptideatlas.org) with a PeptideProphet probability over 0.9. Proteins identified in our experiment but not in the PeptideAtlas database were added to this proteome set (final total: 7454 proteins). To exclude possible biases in sequence or structural properties due to the presence of transmembrane helices, we removed all proteins predicted to contain transmembrane helices using TMHMM v2.0 (Krogh et al., 2001), resulting in 6102 proteins. To prevent bias due to redundancy, we reduced the sequence identity of the set

to 50% using CD-HIT v3.1.1 (Li and Godzik, 2006), resulting in 5637 proteins. These procedures were also applied to our aggregation-prone set and the published set of proteins precipitated by b-isox from U2OS cells. Functional annotation of the aggregation-prone set was done using the freely available DAVID software (http://david.abcc.ncifcrf.gov/). The *C. elegans* proteome set of mass spectrometry detectable proteins was chosen as the background list. GOTERM_BP_FAT and SP_PIR_KEYWORDS were used for the analysis. Redundant categories were removed using the functional annotation clustering option.

Supplemental References:

Boag, P.R., Nakamura, A., and Blackwell, T.K. (2005). A conserved RNA-protein complex component involved in physiological germline apoptosis regulation in C. elegans. Development *132*, 4975-4986.

Brignull, H.R., Morley, J.F., Garcia, S.M., and Morimoto, R.I. (2006). Modeling polyglutamine pathogenesis in C. elegans. Methods in enzymology *412*, 256-282.

David, D.C., Ollikainen, N., Trinidad, J.C., Cary, M.P., Burlingame, A.L., and Kenyon, C. (2010). Widespread protein aggregation as an inherent part of aging in C. elegans. PLoS biology *8*, e1000450.

Hansen, M., Hsu, A.L., Dillin, A., and Kenyon, C. (2005). New genes tied to endocrine, metabolic, and dietary regulation of lifespan from a Caenorhabditis elegans genomic RNAi screen. PLoS Genet *1*, 119-128.

Joeng, K.S., Song, E.J., Lee, K.J., and Lee, J. (2004). Long lifespan in worms with long telomeric DNA. Nature genetics *36*, 607-611.

Krogh, A., Larsson, B., von Heijne, G., and Sonnhammer, E.L. (2001). Predicting transmembrane protein topology with a hidden Markov model: application to complete genomes. Journal of molecular biology *305*, 567-580.

Li, W., and Godzik, A. (2006). Cd-hit: a fast program for clustering and comparing large sets of protein or nucleotide sequences. Bioinformatics *22*, 1658-1659.

Papsdorf, K., Sacherl, J., and Richter, K. (2014). The balanced regulation of Hsc70 by DNJ-13 and UNC-23 is required for muscle functionality. The Journal of biological chemistry *289*, 25250-25261.

Scheckel, C., Gaidatzis, D., Wright, J.E., and Ciosk, R. (2012). Genome-wide analysis of GLD-1-mediated mRNA regulation suggests a role in mRNA storage. PLoS Genet *8*, e1002742.

Schindelin, J., Arganda-Carreras, I., Frise, E., Kaynig, V., Longair, M., Pietzsch, T., Preibisch, S., Rueden, C., Saalfeld, S., Schmid, B., *et al.* (2012). Fiji: an open-source platform for biological-image analysis. Nat Methods *9*, 676-682.

Trinidad, J.C., Thalhammer, A., Burlingame, A.L., and Schoepfer, R. (2013). Activity-dependent protein dynamics define interconnected cores of co-regulated postsynaptic proteins. Molecular & cellular proteomics : MCP *12*, 29-41.

Walther, D.M., Kasturi, P., Zheng, M., Pinkert, S., Vecchi, G., Ciryam, P., Morimoto, R.I., Dobson, C.M., Vendruscolo, M., Mann, M., *et al.* (2015). Widespread Proteome Remodeling and Aggregation in Aging C. elegans. Cell *161*, 919-932.

Yang, J.S., Nam, H.J., Seo, M., Han, S.K., Choi, Y., Nam, H.G., Lee, S.J., and Kim, S. (2011). OASIS: online application for the survival analysis of lifespan assays performed in aging research. PloS one *6*, e23525.